Laser-backscattering imaging for characterising the dairy matrix in different phases during curd processing

Samuel Verdú, Alberto J. Perez, José M. Barat, Raúl Grau

Departamento de Tecnología de Alimentos. Universidad Politècnica de València, Spain

*Author for correspondence: Samuel Verdú

Address: Edificio 8E - Acceso F – Planta 0

Ciudad Politécnica de la Innovación

Universidad Politécnica de Valencia

Camino de Vera, s/n

46022 VALENCIA – SPAIN

E-mail: saveram@upvnet.upv.es

Abstract

The capability of laser-backscattering imaging technique as a non-destructive method to control the effect of fat on curdling process phases was studied. It was based on capturing images of the diffraction patterns generated by a laser-matrix interaction, from which data were acquired. The studied phases were: raw material inspection; curdling monitoring; fresh curd inspection and curd storage monitoring. Milk was used with three different fat contents (0, 1.5 and 3.5%). An extra category of 1.5% fat without lactose was added to test the effect of modification on other compounds. All the phases were characterised by a destructive analysis (rheology, texture profile analysis, syneresis) to study both the evolution of the physical properties during the process and the relation to imaging data. Images successfully captured the variance generated by fat content and physical modifications. Differences in fat content were distinguished for raw material and fresh curd despite lack of lactose. Curdling monitoring also allowed the fat effect to be characterised and coagulation time to be established. Matrix evolution during storage was modelled from imaging for 24 h and 96 h. Imaging data correlated with syneresis evolution and texture features. The obtained results showed that laser-backscattering imaging was capable of capturing the effect of both fat and physical changes on each processing phase, which implies that this technique can be employed as a common system for independent phase control.

Keywords: cheese production; laser backscattering imaging; non-destructive technique; curdling process; monitoring; characterisation; phase change

1. Introduction

Improving food industry processes has favoured developing control procedure efficiency improvements to ensure quality and safety standards. These developments focus on reducing product variability, energy costs and operation times. The aim of the main improvements made to control and inspect modifications is to substitute outdated devices and techniques. Thus adapting new techniques to analyse products and control procedures in different process phases can lead to major short-term improvements without incurring high economic and time costs (Abdul Halim Lim, Antony, Garza-Reyes, & Arshed, 2015; Lim & Antony, 2016). Collecting vast quantities of data from the operations of all process phases is one of the most generalised tendencies of this approach. These data can be managed as databases to improve decision making about any modifications required in real time. This is plausible because the information collected from each process phases can be combined to generate data structures with which new knowledge about the behaviour of the whole production chain can be developed by using automatic learning applications. This approach is performed mainly by devices and techniques that operate non-destructively (Chen, Zhang, Zhao, & Ouyang, 2013; Ropodi, Panagou, & Nychas, 2016). Such techniques need to be based on solid physico-chemical facts from which data are collected, but without coming into contact with the food matrix in any process phase. In addition, the objective entails non-destructive techniques followed to avoid modifications made in places, temperatures, positions, etc. These systems have been successfully applied in the food industry in quality/safety control terms from raw material delivery to end product storage (Arendse, Fawole, Magwaza, & Opara, 2018). The main principles on which those non-destructive techniques are based are ultrasound, light spectroscopy, image analyses, voltametric devices, and combinations of them all (Barbin et al., 2015; Fuentes et al., 2017; Sendin, Manley, & Williams, 2017; Shi et al., 2018; Verdú et al., 2016; Wu et al., 2014; Xie, Chu, & He, 2017; Yang et al., 2018). The main conditional aspects for both the application and development of these techniques are the physico-chemical nature of the selected food matrix and the processing that takes place in each process phase.

A vast number of non-destructive applications have been used in the dairy industry to control most of the phases involved in its processes. Some examples are the detection of microbial contamination and air traces in milk packages with ultrasound (Elvira et al., 2005; Ouacha et al., 2015) and tyramine determination in mouldy cheese based on voltammetric sensors (Küçük & Torul, 2018). Different imaging analysis types have been reported as successful tools to help to control cheese processing: characterisation of curd grain size and distribution (Iezzi et al., 2012), quantification of the amount of rind in grated cheese, (Barreto et al., 2018) starch content determination in adulterated fresh cheese by hyperspectral imaging (Calvini et al., 2020), visualising and modelling the maturity of long-ripening hard cheeses (Priyashantha et al., 2020), etc. In line with this, another imaging technique is laser light backscattering imaging, which has been applied to continuously monitor the cheese curdling process (Verdú et al., 2021). This technique is based on capturing images of the diffraction patterns generated by the interaction between coherent light (laser) and a given matrix. The laser is transmitted through the matrix up to the surface and is scattered because of the sample's internal structure and components. These phenomena may provide information about the structures and morphology of the matrix as backscattered photons inherently interact with internal components (Mollazade et al., 2013). Then scattering properties can be used to study the properties of a matrix, food material in this case (Mireei et al., 2010). Hence this technique's sensitivity and versatility allow normalised information to be taken of the changes made to a matrix in both static and dynamic regimes, and also offers the possibility of being adapted to control the different operations that come into play during a food process with common imaging variables. This technique has been successfully applied to other dairy processes, such as non-destructive yogurt fermentation modelling (Verdú et al., 2019b). Other developed applications in food processing and products include predicting moisture content and colour of bell pepper simultaneously during drying (Romano et al., 2012), quality evaluation of watermelon during storage (Mohd Ali et al., 2017b), predicting the textural properties of vegetable creams (Verdú et al., 2018), modelling the effect of fibre enrichment on biscuit properties (Verdú et al., 2019a), classifying of seeded and seedless watermelons (Mohd Ali et al., 2017a) or characterising antimicrobial particles with essential oils (Verdú et al., 2020).

The objective of this study is to test the capability of laser backscattering imaging to characterise the milk matrix in static and dynamic phases during curd processing as a unique non-destructive control technique.

2. Material and Methods

2.1 Experiment procedure

The experiment focused on testing the capability of laser backscattering imaging to collect useful data from different curd processing phases in order to obtain information about composition and physical properties while manufacturing non-destructively. As the objective was to obtain a common tool to control the entire process, the procedures for extracting and processing images and data were done before destructive analyses and common for all phases, despite it working in the static or continuous mode. In this case, the experiment was carried out using milk with different fat fractions (*Xg*) to evaluate the impact of such composition changes on studying this matrix. Destructive physical analyses were done to acquire information about how both composition and phase modified the matrix, and to then study the relation to the imaging data in each case. Four process points were studied: raw material (liquid milk) inspection; curdling process monitoring; fresh curd inspection; storage monitoring. Raw material inspection was done on four lots of milk with different *Xg* (0, 1.5 and 3.5%): one of 0 and 3.5% *Xg*; two of 1.5% *Xg* of which one lacked lactose. All the phases were analysed by the imaging technique and destructive analyses. Raw material was characterised by static images and rheological analyses. The curdling process was dynamically monitored by the imaging technique and characterised by a rheological analysis to detect the end of the liquid phase and then gel formation. Finished fresh curd was inspected by static imaging, in the same way as with raw material, and in addition to characterisation in textural terms. The changes in matrix during storage were monitored by static imaging, and textural and syneresis measurements were taken at 24 h and 96 h/4ºC.

The destructive analyses and imaging data were singly studied by different statistical analyses. Afterwards, destructive analyses data and imaging data were related to evaluate the relation between both. Then the capability of the imaging technique to capture the variance generated in the milk matrix due to both *Xg* and physico-chemical changes during the process was assessed.

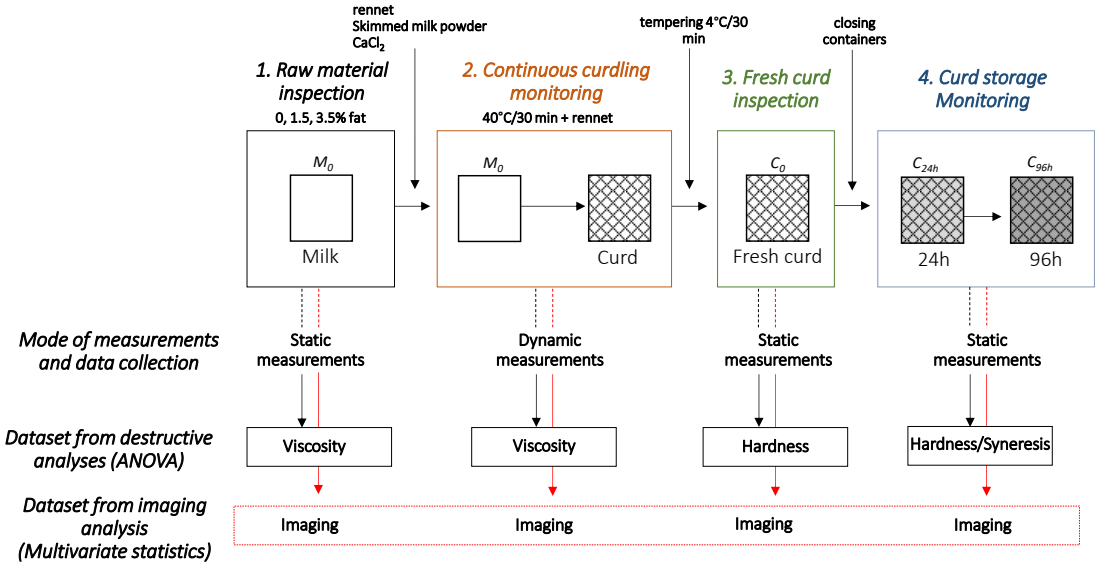

Figure 1. Experiment procedure. Studied curdling process phases and the performed analysis. M_0: raw material/liquid milk; C_0: fresh curd; C_{24h}: curd storage 24 h: C_{96h}: curd storage 9

2.2 Sample preparation in each phase

The raw materials employed for curd formulas were three types of fresh cow's milk with three fat fractions: 0%, 1.5%, and 3.5% fat (*S*, *M* and *W*, respectively). The fractions of protein and carbohydrates were constant for them all: 4.5±0.3% carbohydrates and 3.1±0.3% protein. *A* second *M* category was added, but without lactose (*ML*), to test the effect of *Xg* despite variation in other components. The skimmed milk powder composition was 54±1.5% carbohydrates, 33±1.9% proteins and 1±0.3% lipids. The three milk types and skimmed milk powder were purchased from a local distributor. $CaCl_2$ was supplied by Sigma-Aldrich (Madrid, Spain). The

animal rennet preparation (chymosin 80% w/v, 180 international milk clotting units (IMCU)/ mL) came from the company Productos Nievi S.L. (Biscay, Spain).

The samples for each phase (Figure 1) were prepared as follows:

1. Raw material inspection: milk types were analysed by destructive and imaging techniques at 4ºC with no modifications made to the parameters of the used devices.
    - 50 mL of milk were placed inside two thermoformed polystyrene cylindrical containers (7 cm high, 5.5 cm diameter).
    - The first container was used for the viscosity analysis, and the second for the image analysis.
2. Continuous curdling monitoring: this was carried out with the previously prepared samples.
    - Samples were heated to 40ºC and mixed with the other components of the formula until completely mixed: skimmed milk powder at 1% (w.b., w/v) and 0.15 g of $CaCl_2$ (0.001% w/v).
    - The first container was used for continuous viscosity evolution monitoring, while the second one for continuous imaging evolution monitoring.
    - The curdling process was started by adding two drops of rennet preparation and stirring for 5 sec.
    - Samples were left for 30 minutes at 40ºC to ensure complete phase transition from milk to curd following the rennet provider's instructions. Temperature was maintained in both the rheological and image analysis systems.
3. Fresh curd inspection: in this step, analyses was done on the obtained fresh curd samples
    - Refrigeration of fresh curd during 30 min/4ºC by maintaining the same container.
    - Two containers for the texture analysis and syneresis, and one for the image analysis

4. Curd storage monitoring: this was done with the fresh curd samples in the same containers, which were sealed with plastic film to avoid them drying during this period.
    - Storage was carried out in a refrigerator (Liebherr Mediline) at 4ºC away from light.
    - The analysis times during storage were 24 h and 96 h.
    - Three containers for the analysis at 24 h (texture, syneresis, image), and three at 96 h

The cylindrical shape and selected dimensions of containers allowed a homogeneous heat transfer from the heat exchanger to the matrix, and also avoided containers walls interacting with the laser beam during analyses. The experiment was replicated 10 times per level of *Xg* from 10 different milk lots.

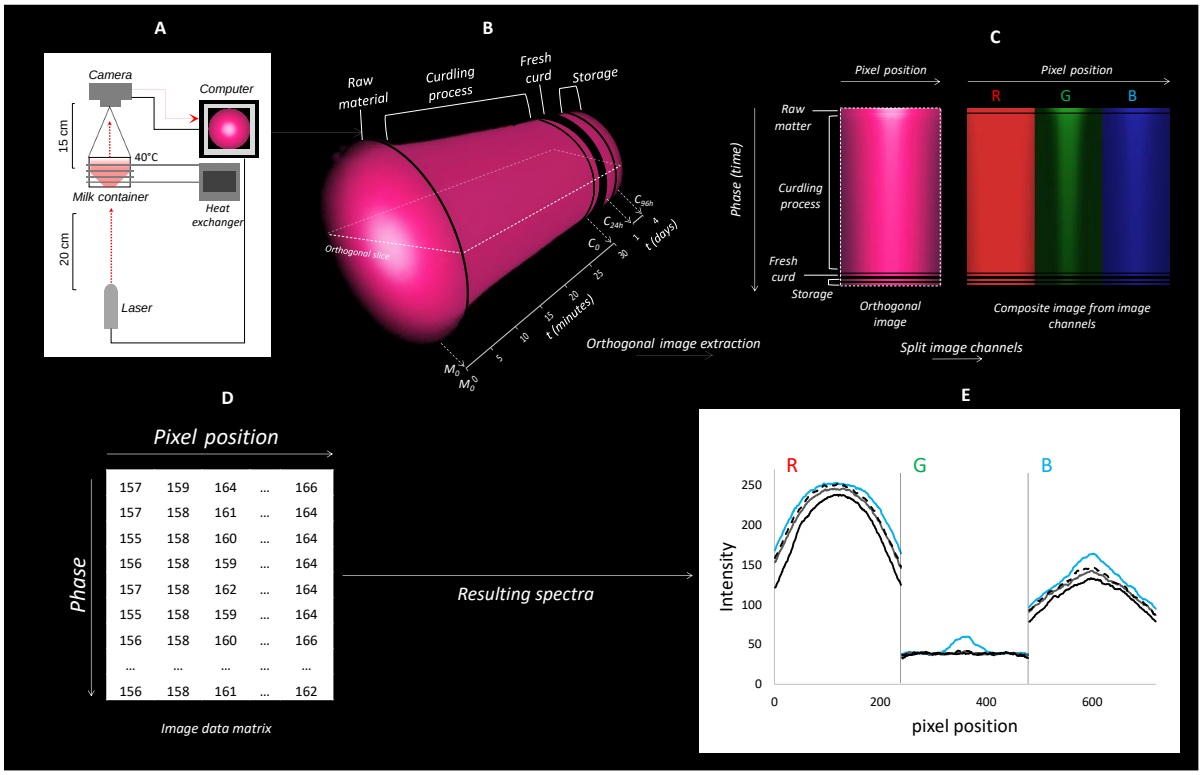

Figure 2. Imaging capture, processing and data extraction. A: Device scheme showing real diffraction patterns; B: Scheme of the resulting time series of the diffraction patterns in each process phase; C: Orthogonal images extracted from each phase in original colours and composite images from split channels R (red), G (green) and B (blue); C: Data matrix extracted from the processed images containing intensity

information; D: Resulting spectral data for statistical studies. M_0: raw material/liquid milk; C_0: fresh curd; C_{24h}: curd storage 24 h: C_{96h}: curd storage 96 h.

2.3 Imaging device

In order to collect information from the images of the different curd processing phases generated by light-matrix interactions, a low-cost device was designed based on coherent light and a digital camera connected to a computer. Figure 2-A offers a scheme of the device setup. The elements were a camera used as the digital capture system, a laser beam, a computer and a heat exchanger for carrying out the curdling process. The setup was installed inside a dark cabin away from light. The capture system was a digital Logitech C920 camera (CMOS sensor, resolution of 2304x1535). All the camera's automatic light controls were set to the manual mode to work and avoid uncontrolled modifications to the capture regime (gain, shutter speed, white balance, etc.). Images were captured in the RGB (red, green and blue) format and were saved as .JPEG (1980x1080). The camera was vertically placed 15 cm over the sample, which lay in the middle of the vision field. The laser beam (650 nm, 50 mW, 3 mm$\varnothing$) was perpendicularly placed 20 cm under the sample container by projecting on the central zone of the bottom surface. The configuration of elements was the same as that employed for analysing samples from all the phases by changing temperature and capture rates depending on whether static or dynamic measurements were required. In the curdling phase, the sample container was coupled to the heat exchanger in the middle of the vision field. Both the laser beam and camera were connected to a conventional computer that ran Linux. This device was used for all the samples in each phase. The only differences were the capture regime and number of images. It was static for raw material, fresh curd and storage, from which one image per sample was captured. For curdling monitoring, the system was controlled by a specific programme that automatically triggered the camera by software to take images at a rate of 1 image/sec. while the milk curdling process was underway (30 min). By the end of the curdling phase, 1,800 images from each sample were obtained. As a result, 1,804 images (raw material= 1; curdling process= 1,800; fresh curd= 1; storage curd 24 h=

1 and storage curd 96 h= 1) from replicates were obtained. Ten replicates per formula from 10 different milk lots were analysed.

2.4 Image processing and data collection

The images captured in the studied process phases were the data reservoir from which the information from milk matrix-laser interactions was collected. The data collection protocol was based on a previous exclusive application for the curdling process with modifications. As explained in Verdú et al., (2021), the protocol was run as follows:

The first step was to create an image stack with the images captured in each phase for every sample category (Figure 2-B). The second step was to extract the orthogonal image from the stack. That image was extracted by slicing the stack across the time axis. Slice size was 50 mm wide (diameter of the sample´s container), which crossed the central zone of the captured diffraction pattern (Fig. 2-B, white line, orthogonal slice). This width corresponded to 180 pixels, which were taken as single variables to collect variance in intensity. Thus any change in light intensity throughout the studied phases was captured in these orthogonal images to simplify the image-stack from 1,804 images to 1 image. The obtained orthogonal image was split in colour channels *R*, *G*, and *B*, from with a composite image was generated (Fig. 2-C). Colour channels were split to collect information from not only *R* pixels, but also from *G* and *B*. In this case, the used wavelength in the laser stimulated the pixels from all the channels because digital cameras do not capture colour in each channel as a particular wavelength of visible light. Typical sensors tend to isolate the *R*, *G* and *B* bands of the visible light spectrum as they are seen by human eyes, but some zones overlapped because laser excites sensors *G* and *B*, albeit less efficiently (Batistell et al., 2014). These zones allow extra data to be collected, which can be useful for this type of imaging processing and analysis applications.

The obtained images contained the intensity profile of the diffraction pattern along the selected pixels from each channel in all phases. Each composite image represented a data matrix of the

changes in the intensity profiles with time (Figure 2-C). The extracted matrix was organised and labelled in a common data matrix to study the evolution of the information captured in each phase, as well as the later relation to the viscosity and textural properties (Fig. 1-D). Thus the data matrix provided spectra of the intensities in each pixel position, which were used as a basis for analytics.

2.5 Destructive analysis

2.5.1 Viscosity measurements

Samples (raw material and the curdling process) were characterised by a rotational viscosimeter (Fungilab EVO Expert Rotational Viscometer, Global Gilson, USA) to measure viscosity. These measurements were based on Ay and Gunasekaran (1994), and taken in the aforementioned thermoformed polystyrene cylindrical containers. A cylinder (2 m diameter), operating at 60 rpm, captured shear stress in mPa.s every second. An analysis was done for 5 min for raw material and for 30 min in the case or curdling phase. Temperature was kept by a tubular heat exchanger connected to an Ultraterm 200 thermostat (JP Selecta, Barcelona, Spain) at 4ºC for raw material and at 40ºC for the curdling process.

2.5.2 Texture measurements

Texture properties were measured in the phases with solid matrix samples: fresh curd and storage curd at 24 h and 96 h. Samples were formed by 50 mL of curd which placed inside thermoformed polystyrene cylindrical containers (7 cm high, 5.5 cm diameter). The curd texture analysis was done with a TA-TX2 texture analyzer (Stable Micro Systems, Surrey, UK), equipped with a 25-kilogram load cell, and was used in an unanalysed sample. A probe with a disc (Ø= 35 mm) operated at constant velocity from 1 mms−1 to 50% of sample depth. The texture study focused on the hardness parameter, which was represented by the maximum resistance during compression measured as g.

2.5.3 Syneresis measurements

Syneresis is the liquid phase migration of a gel because of contraction with no external force applied. It is related to the instability of the network making up the gel, which results in loss of ability to trap or contain serum in the matrix (Walstra, 1993). This phenomenon was analysed in the stored curd in the storage phase at 24 h and 96 h by measuring samples' weight difference after separating the released serum. The result was expressed as a percentage of syneresis (*Sy*), which was calculated according to Equation 1:

$$Sy = \frac{Rs}{M} \quad (1)$$

where *Rs* is the released serum mass during a given period and *M* is the sample's initial mass.

2.6 Statistical analysis

The physical properties of the matrix obtained by destructive analyses were studied by a one-way ANOVA. In those cases in which the effect was significant (P-value < 0.05), means were compared by Fisher's least significant difference (*LSD*) procedure. The imaging technique data were explored after applying multivariable statistical procedures to reduce data-matrix dimensionality. For this purpose, the multivariate unsupervised statistical method called principal component analysis (PCA) was employed. The objective was to simplify the analysis of variance collected by the image data matrix obtained from raw material by continuously monitoring the curdling process and storage. These procedures were run with the *PLS* Toolbox, 6.3 (Eigenvector Research Inc., Wenatchee, Washington, USA), a toolbox extension in the Matlab 7.6 computational environment (The Mathworks, Natick, Massachusetts, USA).

3. Results and Discussion

3.1 Exploring data from destructive analyses

The physico-chemical characterisation results of the matrix in each phases are included in Figure 3. The raw material analysis showed increased viscosity with *Xg* (Figure 3-A). In general, the viscosity of a colloidal suspension increases as the particle concentration rises (McClements et al., 2019). In this case, as the only particle concentrations were fat globules, the observed differences could be exclusively attributed to that modification.

The results about viscosity evolution during the curdling process are included in Figure 3-B. The observed kinetics shows an increase from t= 0 to t~ 1.75 min, which is common for all the sample categories. This point was taken as coagulation time G_t, the time when the sample underwent a phase change. Although the observed peaks coincided for all the samples, the maximum increased viscosities were different following *Xg*, with significant differences between them. In 1.5% *Xg*, the fact that lactose was absent did not generate any differences. This agrees with Hadde et al., (2015), who observed that lactose in milk did not affect the viscosity of fluid in a study about the rheological characterisation of thickened milk components.

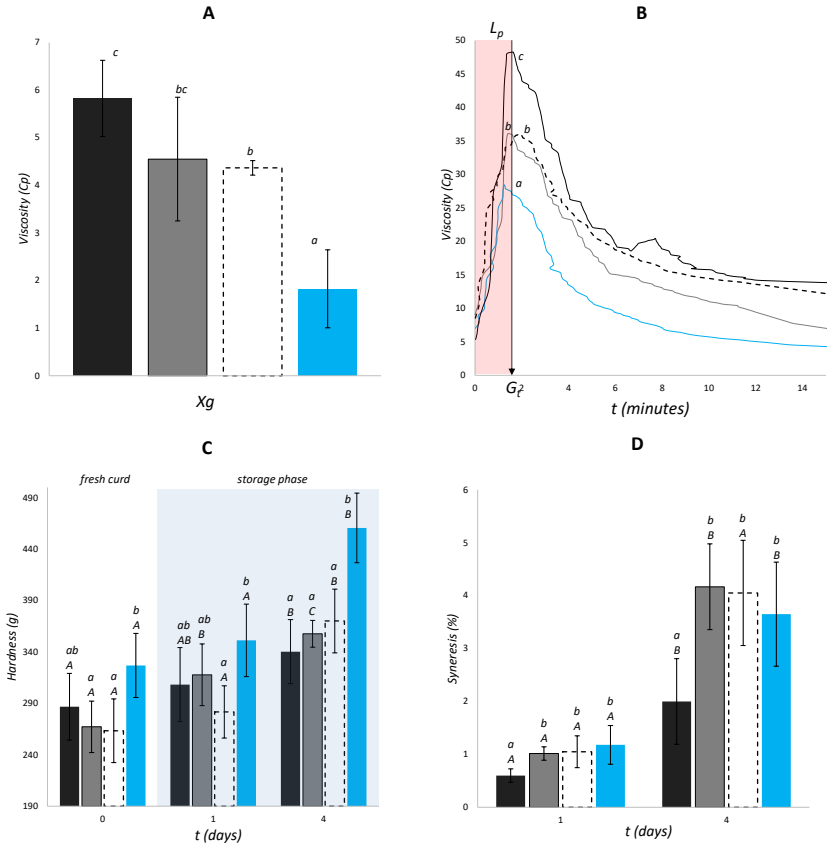

Figure 3. Results of destructive analyses. A: Viscosity in raw material (milks) during the previous curdling process; B: Viscosity evolution during the curdling process. The red zone represents the liquid phase (L_p), arrows denote coagulation time (G_t); C: The texture analysis of fresh curd and storage times (blue zone); D: Syneresis during storage. Black: *W*; Grey: *M*; White-dashes: *ML*; Blue: *S*. Bars indicate standard deviation. Letters denote significant differences at the 95% confidence between categories within a time (lower case letters) and between times (capital letters).

In the L_p, enzymatic activity takes place and modifies the hydrophilic properties of casein micelles. These modifications focus on the surface of casein units via the proteolysis of the Phe_{105}-Met_{106} bonds of κ-casein. This phenomenon induces the destabilisation of colloid and aggregation across three-dimensional spaces to form the gel structure. From this point, values lowered until the end of the analysis. The observed decreased viscosity was due to the effect of the probe on the matrix structure after gelation. Therefore, when casein aggregation sufficed to form a continuous gel, peaks were recorded and then these structures were broken by the device's gyratory movement because solid behaviour was acquired when flux capacity reduced. Hence the effect of *Xg* on viscosity remained after L_p despite changes in the matrix due to enzymes and shear movement.

The fresh curd texture presented significant differences in *Xg*. The highest hardness value was found in *S*, but with no significant differences among the rest. The presence of fat globules in relation to the gel network arrangement during curdling, and subsequent pore size, can modulate the curd structure and, hence, curd texture (Logan et al., 2015). Michalski et al., (2002) reported that fat globules can act disruptively and reduce gel integrity when the pore size of the gel network reduces. Hence the observed results can be attributed to the effect of fat micelles interrupting the casein interaction during the agglomeration process, and then the continuous phase of the formed gel could present less cohesion compared to less *Xg*. This behaviour has been previously reported as lack of fat globules in reduced fat cheese resulted in a firmer texture (Drake et al., 1996; Karaman & Akalin, 2013). Hardness increased during storage in all cases, although S presented the most marked changes, mostly at 96 h. Conversely, water retention in the gel reduced, as shown by the syneresis results (Figure 3-D). This tendency differed at 96 h. A generalised increase took

place and the least marked one was still W, but no differences were observed for the other categories. Increased hardness is related to the contact dynamics between casein micelles over time. The number of bonds per casein unit junction increases with ageing (Fagan et al., 2017). Micelles have a given fusion level in a fresh curd matrix. After some hours however, the original particles making up the gel can no longer be distinguished, and firmness increases with time (van Vliet et al., 1991). This phenomenon produces the progressive and spontaneous retraction of the protein matrix at low storage temperature, which allows water with hydro-soluble compounds to escape. Thus the rearrangement of the matrix network causes syneresis to increase. These texture modifications to this matrix during ripening are also related to proteolysis, along with changes in the matrix structure's water-binding ability. In this case however, it can be neglected because chymosin is inactive at temperatures below 15ºC (Ardö et al., 2017).

3.2 Exploring imaging data

After acquiring the images from each studied phase, data were extracted and processed following the above-mentioned procedure. Some examples of images from each phase and *Xg* are included in Figure 4 to display the effect of the studied factors on the generated diffraction patterns captured during the experiment. A matrix formed by the raw images of sample surfaces is included in Figure 4-A. The columns of that matrix represent time evolution, divided into the studied phases: raw material M_o; fresh curd C_o; stored curd 24 h (C_{24h}) and stored curd 96 h (C_{96h}). Rows represent increased *Xg*. Figure 4-B shows the matrix of images after splitting colour channels (*RGB*). In addition, the intensity profiles of each diffraction pattern are included to numerically visualise the observed differences. The generated diffraction patterns presented two differentiable zones: a central zone with higher intensity, from which a second zone was generated and corresponded to the most diffracted laser beam fraction. This structure has been previously studied to model other matrix types like biscuits and yogurt (Verdú et al., 2019b, 2019a). The effect of *Xg* was observed on these properties of the diffraction pattern. Light transmittance lowered because of the intense zone reduced with increasing *Xg* in all the process phases, while storage time had the opposite

effect. This effect was better evidenced in the *G* channel. The central zone transmitted more radiation to the camera´s sensor by stimulating not only the *R* pixels, but also the *G* and *B* ones.

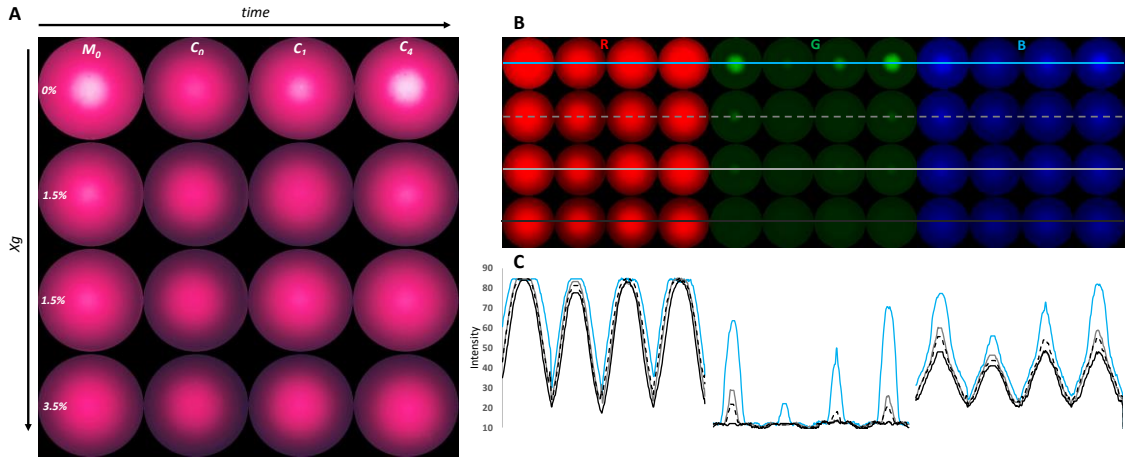

Figure 4. Examples of the diffraction patterns from the whole process. A: Matrix of diffraction patterns obtained from each process phase, the X-axis marks time and the Y-axis denotes Xg. B: Composite image from the matrix's RGB channels. Lines indicate the extraction zone of the intensity data; C: Spectra of the intensity data from the shown images. Black: W; Grey: M; White-dotted: ML; Blue: S

The presence of fat globules increased the light-matrix interaction in both the liquid and solid states, with a smaller diffraction pattern in all cases (Figure 5-A). The basis of this effect as regards the light interaction in the dairy matrix, measured by some light-based techniques, has been previously reported by several authors, who indicate increased turbidimetry and refractive indices (Penchev et al., 2015). The structural modifications that occurred in the matrix during both the curdling and storage processes also altered the light-matrix interaction. The reduced transmittance observed after the curdling process (fresh curd C_0) evidenced changes in the matrix due to the proteolysis and aggregation of casein micelles (Figure 5-B). From this point, transmittance seemed to once again increase with storage time. The images from the storage phase (Figure 4, columns C1 and C4) showed this increase. It can be explained by the local deformation or breakage of the casein structures that formed during the curdling process, which underwent modifications, including compaction and structural loss in localised zones. Thus after evidencing the dependence of the diffraction pattern structures from the studied factors, images were

processed, and data were extracted and arranged, to study each process phase with the corresponding statistical procedures.

3.2.1 Raw material inspection

The first step was to characterise raw material after the curdling process in order to test the influence of *Xg* on the light-matrix interaction of milk, and then how the information captured by the imaging technique would be conditioned by this factor. For this purpose, dimensionality was reduced by means of *PCA* from the spectra obtained from the images corresponding to the raw material of all the *Xg*. Figure 6-A shows the space of variance delimited by *PC1* and *PC2*. Samples were spontaneously clustered following an increase in *Xg* across *PC1*. Thus *PC1* collected the variance generated in the diffraction patterns captured in the images given the differences in *Xg*. Note how the samples from *ML* are placed in the same zone of *M* according to the common *Xg* for both sample categories. In this case, apparently the differences in composition in lactose terms did not generate enough variance in the captured data because *M* samples overlapped in this space of variance. The observed placement was in accordance with the above-mentioned differences, which are observed in the raw data shown in Figure 4. In addition, when the correlation study between the average of the *PC1* scores and the viscosity data of raw material (Figure 3-A) was carried out, r= 0.95 was obtained, which evidenced the previously observed dependence. Therefore, the differences in the *Xg* of raw material were significantly affected in the data captured by the imaging technique, a phenomenon from which the non-destructive characterisation of different milk types can be carried out before the curdling process.

3.2.2 Continuous curdling process monitoring

The effect of *Xg* on monitoring the milk curdling phase was studied by the same procedure, but using the data from the images captured in the dynamic mode throughout the process. The time series of the images from all the sample categories was joined in stacks and a *PCA* was used to

reduce the dimensionality of the resulting data matrix. The result of generating the space of variance is included in Figure 7-A, where the *PC1* collected 89% of total variance. The *PC1* scores were plotted with time to observe data evolution throughout the phase. The sample categories showed very similar evolution over time, with the main difference lying in the position at t= 0. At the beginning of the process, samples were placed following *Xg*, like that previously observed in the raw material characterisation. From this point, evolution seemed parallel for them all up to t= 30min, which was the end of the process, although some differences were noted. These differences were observed in segments t= 0 and t= 1min. The observed slopes differed between *Xg*, although a change in tendency occurred at the same time. In this case, *PC1* collected both the variance generated by *Xg* and rennet enzymes in this phase. Two zones were differentiated during the process based on change in slope. However, it was difficult to determine the matrix's gelation (G_t) time. In order to amplify the change in tendency and to determine the instant when data generated the change in evolution, the *PC1* scores were transformed into the first derivative. Figure 7-B shows the first derivative of the scores from *PC1*, where a peak for all the categories is observed at the same time. This confirmed a change in matrix behaviour at around t= 1.75 min, which coincided with that observed in the rheological measurements. The relation between the values of the observed peaks in the first derivative of the scores from PC1 and the viscosity data at *Gt* reported r= 0.97, which confirmed the above-observed covariance.

The differences in *PC* behaviour allowed us to relate differences to several diffraction pattern zones, which could explain the effect of proteolysis and aggregation on the light-matrix interaction. These results agree with former curdling process modelling in Verdú et al., (2021), where this imaging technique allowed the curdling phase between milk with different dry fractions to be characterised. It showed how intensity reduced due to the increasing interaction of light with the casein network structures, and despite the differences in *Xg*. These phenomena have also been described by the classic light backscattering method to study the curdling process in a laboratory, where reduced light transmittance was also detected during milk curdling by spectroscopic techniques (Mateo et al., 2010).

Although *Xg* generated significant differences in the captured diffraction patterns because of the influence on the light-matrix interaction, the variance generated by proteolysis and caseins aggregation allowed successful curdling phase monitoring for all the sample categories and G_t was determined.

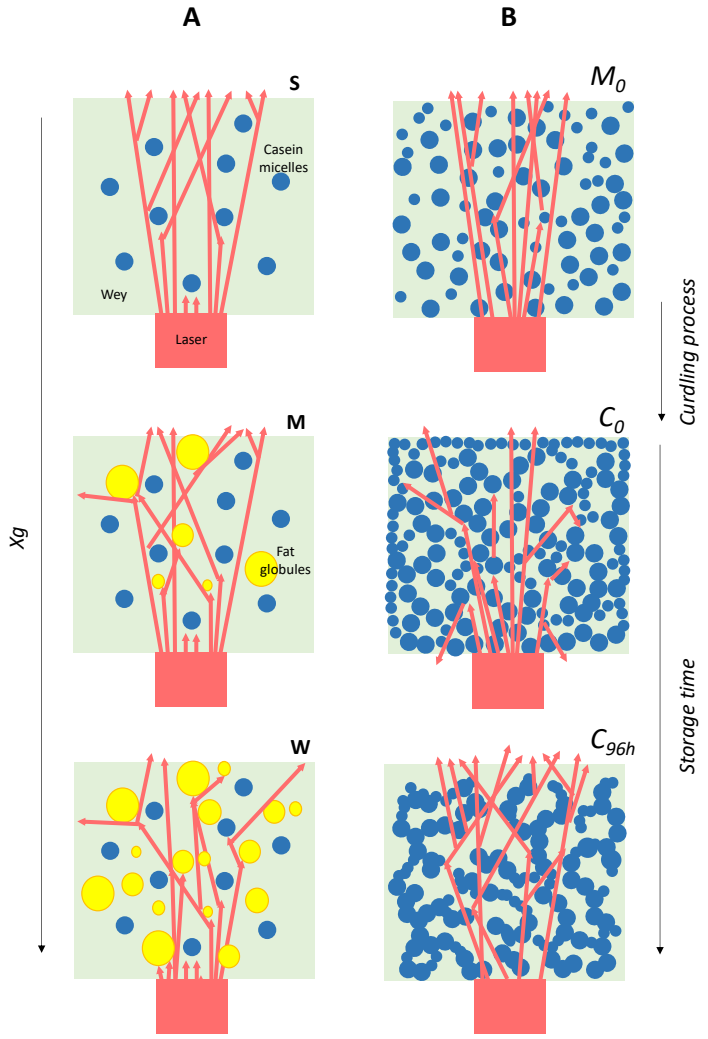

Figure 5. Scheme of the laser-matrix interaction with the studied factors. A: effect of a fat globule; B: effects of gelation and gel restructuration during storage.

3.2.3 Fresh curd inspection

The fresh curd samples (C_0) were characterised with the imaging device after the curdling process and tempering for 30 min at 4ºC. The collected data were analysed by a *PCA*. The resultant space of variance in shown in Figure 6-B. Sample coordinates displayed similar behaviour to the raw material one. The distribution of samples maintained the clusters corresponding to the used categories based on *Xg*. After the gelation and refrigeration of the matrix, the interaction of the gel structure with the laser beam allowed the variance captured in the raw material analysis to remain due to the differences in *Xg*, albeit with a generalised reduction in transmittance. This result followed the differences observed during the curdling process at the end of the phase (Figure 7-A) when, although the curdling kinetics was almost equal, differences in intensity between *Xg* were observed. So although the biochemical modifications that occurred during the curdling process generated significant variance in the state and structure of the matrix, the variance generated by *Xg* still represented a wide fraction of the total captured by images. That fraction of variance was enough to differentiate fresh curds non-destructively.

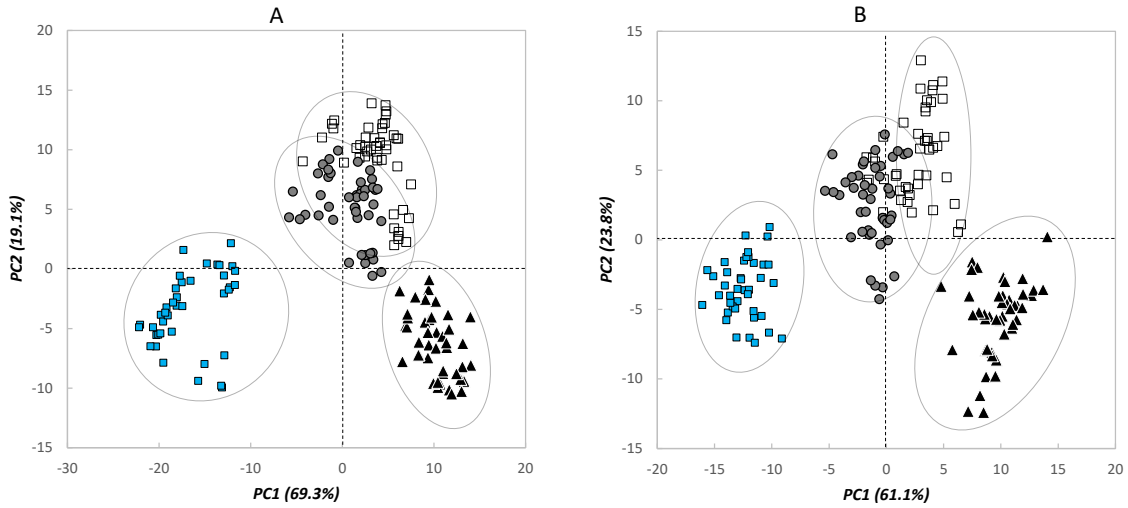

Figure 6. Results of the characterisation of milk (A) and fresh curd (B) using imaging data after dimensionality reduction by PCA. Black triangles: W; Grey circles: M; White squares: ML; Blue squares: S.

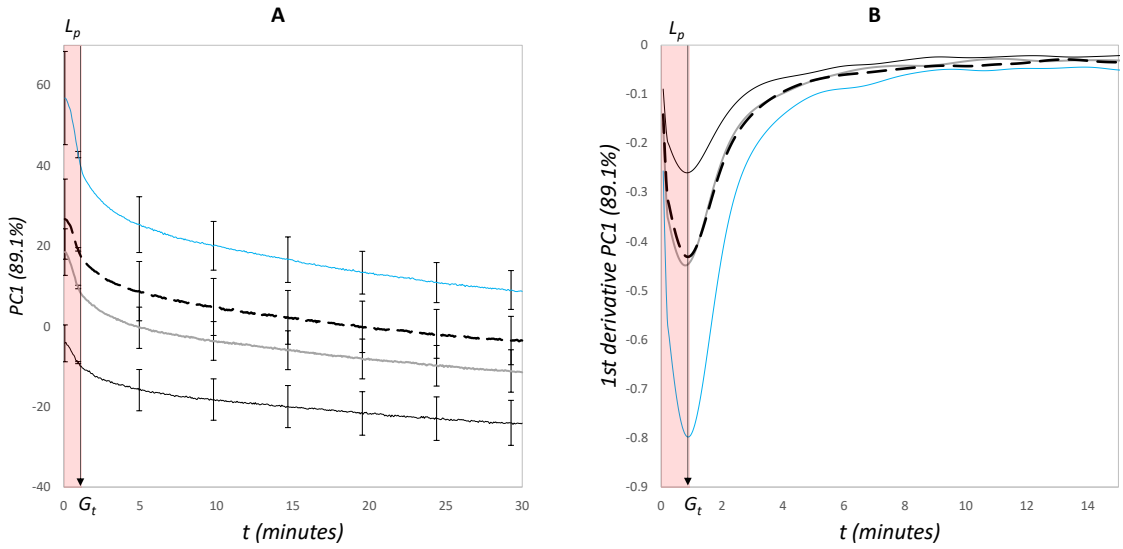

Figure 7. The curdling process study results with the imaging data. A: PC1 evolution according to a PCA over curdling time for all categories; B: Transformed PC1 scores from a common PCA as the first derivative. Red zone represents the liquid phase (L_p), arrows mark the coagulation time (G_t). Black: W; Grey: M; black dotted: ML; Blue: S.

3.2.4 Curd storage monitoring

Fresh curd characterisation during storage at 4ºC was carried out by statically capturing images at 24 h and 96 h. The results were compared to those of fresh curd to characterise the captured data evolution and to evidence the observed matrix evolution in the previously presented physical characterisation. Figure 8 shows the average of the raw intensity data for each colour channel and all the milk categories at each time. Generally for this phase, spectra once again showed bigger differences with time for channels *G* and *B*. Storage time seemed to increase matrix transmittance, unlike *Xg*, which had the opposite effect. Thus although the matrix underwent changes during storage, which generated differences in the diffraction patterns, the change in variance generated by *Xg* remained during the study period. Moreover, transmittance varied less over storage time when fat was present in the matrix (Figure 8-D). This matched the texture and syneresis results, which also showed fewer changes following the increase in *Xg*. This confirmed how fat induced

a stabler matrix during storage. If it is considered the compaction previously evidenced with increased hardness, then the observed effect of time on transmittance was not expected. This can be explained by the previous results of several authors. Rearrangements of casein micelles during storage modifies the curd matrix, and it becomes a more compact structure because the number of bonds increases and, hence, the system's total free energy decreases (see Figure 5B, storage time). As casein structures form part of the gel network, it must be deformed or break locally to form new junctions (Ardö et al., 2017; Walstra, 1993). Thus an increase in local breaks during storage can explain the increasing intensity observed in C_{24h} and C_{96h} due to discontinuities being generated across the gel.

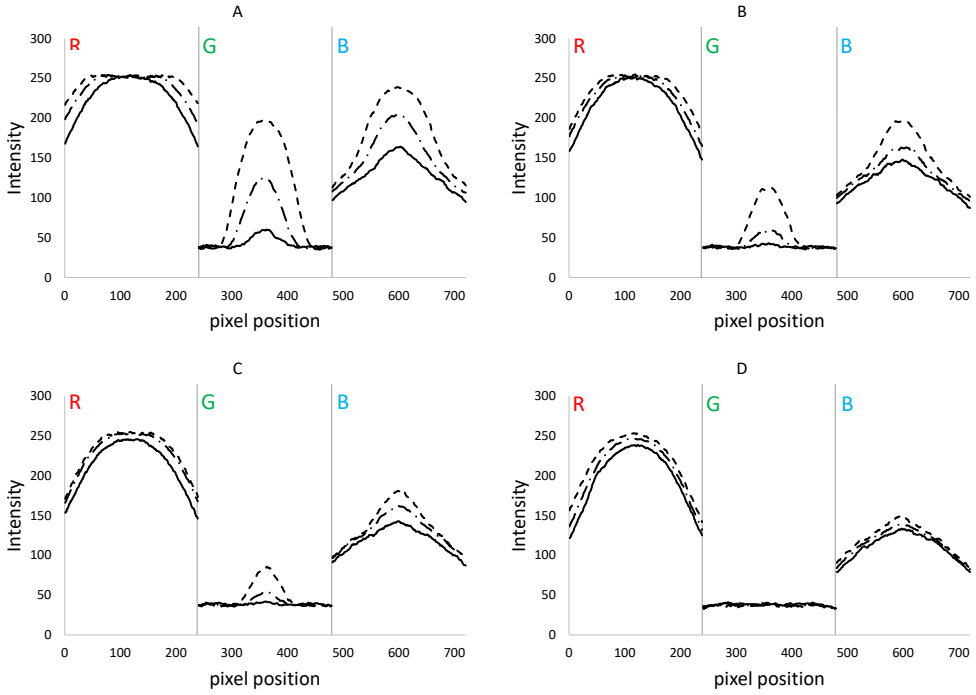

Figure 8. Raw intensity spectra from the processed images over storage time. A: *S*; B: *M*; C: *ML*; D: *W*. Image channels: *R* (red), *G* (green), *B* (blue). Continuous line: C_0; semi-dotted line: C_{24h}; dotted line: C_{96h}

All the imaging data obtained from storage were processed by *PCA* to reduce dimensionality. The generated space of variance showed a spontaneous order of sample categories with time and *Xg*. Figure 9-A depicts the space of variance generated between *PC1* and *PC2*, where the averages of scores are represented to improve the visualisation of coordinates.

The placement of categories followed both *Xg* and storage time, from which it was possible to determine each one across the axis, although no factor was attributed to any *PC* because the observed models presented diagonal tendency. Note how *M* and *WL* were placed without differences. Thus the generated space of variance collected the effect of both *Xg* and storage time, from which the differentiation of each category of samples at several storage times can be done. Direct relations were observed when the imaging data dimensionally reduced as *PC1* correlated with hardness and syneresis. Figure 9-B shows a 3D-plot with that relation. The imaging data showed a positive relation with hardness and syneresis. The results revealed a direct relation between the imaging data and matrix evolution in hardness and syneresis terms, which evidences the imaging technique's capability to control and characterise the evolution of gel stability and textural properties during a given storage.

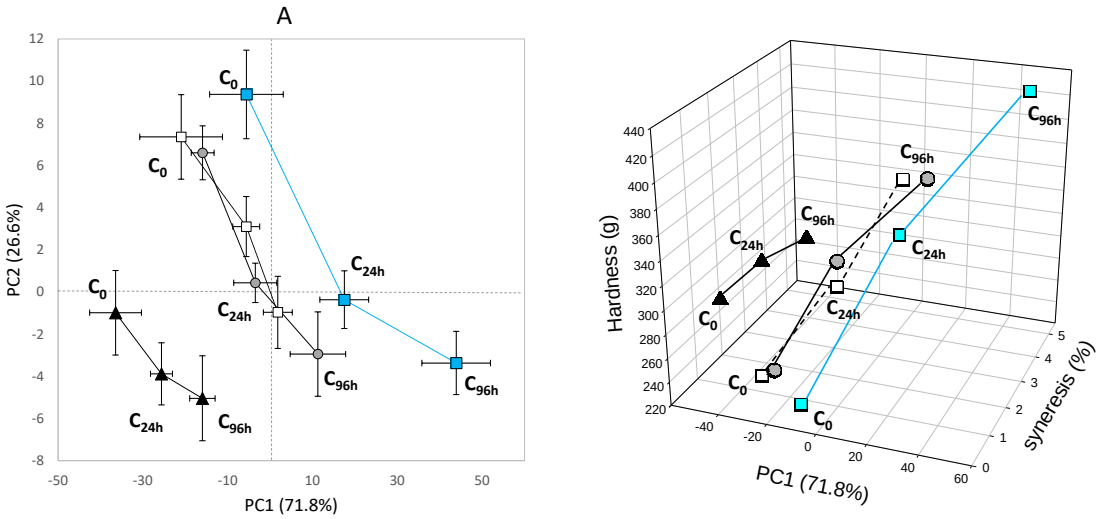

Figure 9. Results of imaging data studies from storage time. A: Space of variance of a PCA from the imaging data from all the sample categories on C_0, C_{24h} and C_{96h}; B: Relation of texture and syneresis results with imaging data after dimensionally reduction via PCA. Black triangles: *W*; Grey circles: *M*; White squares: *ML*; Blue squares: *S*. Bars indicate standard deviation.

4. Conclusions

The laser-backscattering imaging technique can be applied as a tool to characterise and control the effect of fat content on different curd processing phases. The technique captured data from which variance generated because both the fat content and physical modifications of the dairy matrix were studied and modelled. The effect of fat content can be characterised in all the studied phases despite modifications in other components, such us lactose. Moreover, continuous curdling process monitoring allowed the characterisation of the effect of fat quantity and proteolysis/aggregation phenomena of casein micelles across time. With this information, the end of the liquid phase can be detected in real time, and then the coagulation time can be established. Data evolutions continued to correlate with the evolution of the syneresis and texture features of each fat content during storage. This means that the obtained results showed the imaging technique's capability to non-destructively capture the produced variability because of the composition modifications, fat in this case, in each curdling processing phase. These features offer the possibility of using this technique as a common data collection system for the entire process regardless of the phase or physical state of the matrix.

5. Acknowledgement

The authors gratefully acknowledge financial support from the Universitat Politècnica de València.

6. Bibliography

Ardö, Y., McSweeney, P. L. H., Magboul, A. A. A., Upadhyay, V. K., & Fox, P. F. (2017). Biochemistry of Cheese Ripening: Proteolysis. In *Cheese: Chemistry, Physics and Microbiology: Fourth Edition*. https://doi.org/10.1016/B978-0-12-417012-4.00018-1

Barreto, A., Cruz-Tirado, J. P., Siche, R., & Quevedo, R. (2018). Determination of starch content in adulterated fresh cheese using hyperspectral imaging. *Food Bioscience*.

https://doi.org/10.1016/j.fbio.2017.10.009

Batistell, G., Zhang, V. C., & Sturm, J. (2014). Color recognition sensor in standard CMOS technology. *Solid-State Electronics*. https://doi.org/10.1016/j.sse.2014.06.002

Calvini, R., Michelini, S., Pizzamiglio, V., Foca, G., & Ulrici, A. (2020). Exploring the potential of NIR hyperspectral imaging for automated quantification of rind amount in grated Parmigiano Reggiano cheese. *Food Control*. https://doi.org/10.1016/j.foodcont.2020.107111

Drake, M. A., Herrett, W., Boylston, T. D., & Swanson, B. G. (1996). Lecithin improves texture of reduced fat cheeses. *Journal of Food Science*. https://doi.org/10.1111/j.1365-2621.1996.tb13176.x

Elvira, L., Sampedro, L., Matesanz, J., Gómez-Ullate, Y., Resa, P., Iglesias, J. R., Echevarría, F. J., & Montero De Espinosa, F. (2005). Non-invasive and non-destructive ultrasonic technique for the detection of microbial contamination in packed UHT milk. *Food Research International*. https://doi.org/10.1016/j.foodres.2004.12.001

Fagan, C. C., O'Callaghan, D. J., Mateo, M. J., & Dejmek, P. (2017). The Syneresis of Rennet-Coagulated Curd. In *Cheese: Chemistry, Physics and Microbiology: Fourth Edition*. https://doi.org/10.1016/B978-0-12-417012-4.00006-5

Hadde, E. K., Nicholson, T. M., Cichero, J. A. Y., & Deblauwe, C. (2015). Rheological characterisation of thickened milk components (protein, lactose and minerals). *Journal of Food Engineering*. https://doi.org/10.1016/j.jfoodeng.2015.06.016

Iezzi, R., Locci, F., Ghiglietti, R., Belingheri, C., Francolino, S., & Mucchetti, G. (2012). Parmigiano Reggiano and Grana Padano cheese curd grains size and distribution by image analysis. *LWT - Food Science and Technology*. https://doi.org/10.1016/j.lwt.2012.01.035

Karaman, A. D., & Akalin, A. S. (2013). Improving quality characteristics of reduced and low fat Turkish white cheeses using homogenized cream. *LWT - Food Science and*

Technology. https://doi.org/10.1016/j.lwt.2012.08.017

Küçük, A., & Torul, O. (2018). Voltammetric sensor based on poly(3-methylthiophene) synthesized in dichloromethane for tyramine determination in moldy cheese. *Synthetic Metals*. https://doi.org/10.1016/j.synthmet.2018.01.009

Logan, A., Leis, A., Day, L., Øiseth, S. K., Puvanenthiran, A., & Augustin, M. A. (2015). Rennet gelation properties of milk: Influence of natural variation in milk fat globule size and casein micelle size. *International Dairy Journal*. https://doi.org/10.1016/j.idairyj.2014.08.005

Mateo, M. J., O'Callaghan, D. J., Everard, C. D., Castillo, M., Payne, F. A., & O'Donnell, C. P. (2010). Evaluation of on-line optical sensing techniques for monitoring curd moisture content and solids in whey during syneresis. *Food Research International*. https://doi.org/10.1016/j.foodres.2009.09.023

McClements, D. J., Newman, E., & McClements, I. F. (2019). Plant-based Milks: A Review of the Science Underpinning Their Design, Fabrication, and Performance. In *Comprehensive Reviews in Food Science and Food Safety*. https://doi.org/10.1111/1541-4337.12505

Michalski, M. C., Cariou, R., Michel, F., & Garnier, C. (2002). Native vs. damaged milk fat globules: Membrane properties affect the viscoelasticity of milk gels. *Journal of Dairy Science*. https://doi.org/10.3168/jds.S0022-0302(02)74327-0

Mireei, S. A., Mohtasebi, S. S., Massudi, R., Rafiee, S., & Arabanian, A. S. (2010). Feasibility of near infrared spectroscopy for analysis of date fruits. *International Agrophysics*, *24*(4), 351–356. https://www.scopus.com/inward/record.uri?eid=2-s2.0-79955023784&partnerID=40&md5=bda54a95925b007416fe8354a2214b79

Mohd Ali, M., Hashim, N., Bejo, S. K., & Shamsudin, R. (2017a). Laser-induced backscattering imaging for classification of seeded and seedless watermelons. *Computers and Electronics in Agriculture*, *140*, 311–316. https://doi.org/10.1016/j.compag.2017.06.010

Mohd Ali, M., Hashim, N., Bejo, S. K., & Shamsudin, R. (2017b). Quality evaluation of watermelon using laser-induced backscattering imaging during storage. *Postharvest Biology and Technology*, *123*, 51–59. https://doi.org/10.1016/j.postharvbio.2016.08.010

Mollazade, K., Omid, M., Akhlaghian Tab, F., Kalaj, Y. R., Mohtasebi, S. S., & Zude, M. (2013). Analysis of texture-based features for predicting mechanical properties of horticultural products by laser light backscattering imaging. *Computers and Electronics in Agriculture*, *98*, 34–45. https://doi.org/10.1016/j.compag.2013.07.011

Ouacha, E., Faiz, B., Moudden, A., Aboudaoud, I., Banouni, H., & Boutaib, M. (2015). Non-destructive detection of air traces inside UHT milk package by using ultrasonic through transmission method. *International Review of Mechanical Engineering*. https://doi.org/10.15866/ireme.v9i6.7798

Penchev, E. V., Bock, W. J., Eftimov, T. A., & Mikulic, P. (2015). Using double resonance long period gratings to measure refractive index of milk of varying fat content. *Bulgarian Chemical Communications*.

Priyashantha, H., Höjer, A., Saedén, K. H., Lundh, Å., Johansson, M., Bernes, G., Geladi, P., & Hetta, M. (2020). Use of near-infrared hyperspectral (NIR-HS) imaging to visualize and model the maturity of long-ripening hard cheeses. *Journal of Food Engineering*. https://doi.org/10.1016/j.jfoodeng.2019.109687

Romano, G., Argyropoulos, D., Nagle, M., Khan, M. T., & Müller, J. (2012). Combination of digital images and laser light to predict moisture content and color of bell pepper simultaneously during drying. *Journal of Food Engineering*, *109*(3), 438–448. https://doi.org/10.1016/j.jfoodeng.2011.10.037

van Vliet, T., van Dijk, H. J. M., Zoon, P., & Walstra, P. (1991). Relation between syneresis and rheological properties of particle gels. *Colloid & Polymer Science*. https://doi.org/10.1007/BF00659917

Verdú, S., Barat, J. M., & Grau, R. (2019a). Laser backscattering imaging as a non-destructive quality control technique for solid food matrices: Modelling the fibre enrichment effects on the physico-chemical and sensory properties of biscuits. *Food Control*. https://doi.org/10.1016/j.foodcont.2019.02.004

Verdú, S., Barat, J. M., & Grau, R. (2019b). Non destructive monitoring of the yoghurt fermentation phase by an image analysis of laser-diffraction patterns: Characterization of cow's, goat's and sheep's milk. *Food Chemistry*, *274*(July 2018), 46–54. https://doi.org/10.1016/j.foodchem.2018.08.091

Verdú, S., Pérez, A. J., Barat, J. M., & Grau, R. (2018). Laser backscattering imaging as a control technique for fluid foods: Application to vegetable-based creams processing. *Journal of Food Engineering*, *241*(May 2018), 58–66. https://doi.org/10.1016/j.jfoodeng.2018.08.003

Verdú, S., Pérez, A. J., Barat, J. M., & Grau, R. (2021). Non-destructive control in cheese processing: Modelling texture evolution in the milk curdling phase by laser backscattering imaging. *Food Control*. https://doi.org/10.1016/j.foodcont.2020.107638

Verdú, S., Ruiz-Rico, M., Pérez, A. J., Barat, J. M., & Grau, R. (2020). Application of laser backscattering imaging for the physico-chemical characterisation of antimicrobial silica particles functionalised with plant essential oils. *Journal of Food Engineering*. https://doi.org/10.1016/j.jfoodeng.2020.109990

Walstra, P. (1993). The Syneresis of Curd. In *Cheese: Chemistry, Physics and Microbiology*. https://doi.org/10.1007/978-1-4615-2650-6_5